SIMULATION OF ORTHOGONAL THREE-DIMENSIONAL WOVEN CARBON PLATES UNDER BALLISTIC IMPACT

Tao Liu[1], Paul Turner[2], Xuesen Zeng

[1]Centre for Structural Engineering and Informatics, Composites Research Group, Faculty of Engineering, University of Nottingham, University Park, Nottingham, NG7 2RD, U.K.
Email: Tao.Liu@nottingham.ac.uk

[2]Centre for Structural Engineering and Informatics, Composites Research Group, Faculty of Engineering, University of Nottingham, University Park, Nottingham, NG7 2RD, U.K.

[3]Composites Research Group, Faculty of Engineering, University of Nottingham, University Park, Nottingham, NG7 2RD, U.K.

Keywords: 3D woven composite plate, ballistic impact, Finite elements, penetration

ABSTRACT

Finite element simulations were conducted to investigate the dynamic response of a clamped orthogonal 3D woven carbon circular plate under singular ballistic impact with focus on the role of the through-the-thickness (TTT) reinforcement. The presence of the TTT-reinforcement caused an 8% increase in the predicted ballistic limit of the composite plate, i.e. an increase from V_L = 152.5 ms^{-1} without TTT reinforcement to V_L = 165.0 ms^{-1} inclusive of TTT reinforcement. With the presence of the TTT reinforcement, stress transferal from the in-plane fibre architecture to the through-thickness reinforcement was demonstrated. This causes a significant reduction in in-plane longitudinal tensile stress throughout the plate, and also local reductions in stress at the positions of the TTT reinforcement. The tensile fibre damage was predicted to propagate more significantly in the direction of the TTT reinforcement for the 3D woven sample (with TTT reinforcement), and along the in-plane fibre orientation for the equivalent UD-laminate (without TTT reinforcement). Predictions of both the 3D woven and equivalent UD-laminate material reveal a progressive increase of inelastic processes, predominantly of material damage, with increasing velocity of projectile impact. The 3D woven material is shown to have approximately a 25% increase in the coefficient of restitution in comparison with the equivalent UD-laminate material within the normalised projectile velocity range: $0.35 \le \bar{v}_0 \le 0.85$, where $\bar{v}_0 \equiv v_0 / V_L$, and V_L is the ballistic limit.

1 INTRODUCTION

The high specific stiffness and strength of fibre reinforced composite materials, combined with their low coefficient of thermal expansion, are excellent incentives for their use within protective systems for highly mobile vehicles. The dynamic impact of debris upon aircraft systems is of great concern and is often a critical load case for design engineers to consider. Common sources of impact events for aeronautical structures include hail stones, bird strikes, and runway debris. The first two of these impact systems are classified as soft body impact, the third is that of solid projectiles. During take-off and landing, aircrafts can receive impact events from runway debris at velocities up to approximately 250 ms^{-1} [1]. These impacts can cause damage to the fibre reinforcement, the matrix material and can introduce delamination damage within laminate composites.

Extensive research into 3D woven composite materials has demonstrated the scenarios that revealed the advantages of 3D woven composites over UD-laminate or 2D woven composites, see Mouritz et al. [2]. For example, the inter-laminar fracture toughness values of 3D woven composites have been reported in the literature up to values as high as 7000 J/m^2, with far less reductions of in-plane material properties as is common with 2D woven structures. For soft body impact, Turner et al. [3] experimentally and numerically investigated the dynamic behaviours of clamped orthogonal 3D

woven carbon composite beams under metal foam projectile soft impact at the velocities up to 270 ms^{-1}. The results suggested that the 3D woven carbon composite beams had much less in-plane damage and delamination damage compared to the equivalent UD-laminate beams. In this paper, numerical simulations were conducted to understand the failure mechanism of an orthogonal three-dimensional woven carbon plate under ballistic impact with focus on the role of the through-the-thickness (TTT) reinforcement.

2 MATERALS

An orthogonal 3D woven carbon fibre epoxy resin composite material was manufactured using the method described by Turner et al. [3]. The material contained an alternating stack of 9 weft layers and 8 warp layers. Top and bottom tows were orientated along the weft direction, and were the only tows with an induced crimp due to localised influence of the TTT-reinforcement. The geometry of the cured composite material is shown in Fig.1. The average width and thickness of warp tows were 1.70 mm and 0.177 mm, respectively. The average width and thickness of weft tow were 1.40 mm and 0.230 mm, respectively. The average width and thickness of TTT-reinforcement were 0.5 mm and 0.1 mm, respectively. Spacing between TTT-reinforcement was 3.48 mm. Total fibre volume fraction for the cured composite was 0.55. The tow fibre volume fractions, i.e. the ratio of the area of fibres into the area of the tow, were 0.785, 0.692, and 0.795 for warp, weft, and TTT-reinforcement tows, respectively. A co-ordinate system is defined in Fig. 1 and utilised throughout this paper: the direction running parallel to the warp tows is referred to as x-direction, the direction running parallel to the weft tows as y-direction, and the though-thickness direction is referred to as the z-direction. Quasi-static (2mm /min) uniaxial coupon tests were conducted on the composite material using the procedure detailed by Turner et al. [3]. Figure 2 (a) and (b) present the tensile and compressive stress-strain curves of the 3D woven carbon composite material.

3 FINITE ELEMENT SIMULATION

The 3D woven carbon composite material was modelled using the method described by Turner et al. [3]. The three-dimensional (3D) finite model was created within the ABAQUS (Version 6.12) explicit solver. Each of the 17 layers of the composite material as well as the TTT reinforcement were modelled separately using 4-noded doubly curved reduced integration shell elements (S4R in ABAQUS notation), with 5 integration points through the thickness, see Fig.3. The element size for the laminate was approximately 800 μm. The constitutive models for fibre reinforced composites of Hashin [4] and Matzenmiller et al. [5] were employed with material parameters extracted from uniaxial coupon tests, see [3]. The translation and rotational degrees of freedom were constrained around the peripheral of all the layers. The layers were joined together through the thickness with a cohesive interaction. The stainless steel projectile consisted of a stainless steel sphere of diameter d_p = 12.7 mm and mass m_p = 8.3 g. The projectile was assumed to incur negligible deformation throughout the penetration event, and was modelled as a discrete rigid body (C3D8R in ABAQUS notation). The mass of the projectile was assigned by the inertial assignment function within ABAQUS, at the centre of the projectile. Penalty based contact method with general contact option within ABAQUS was used to simulate the interaction between the projectile and plates.

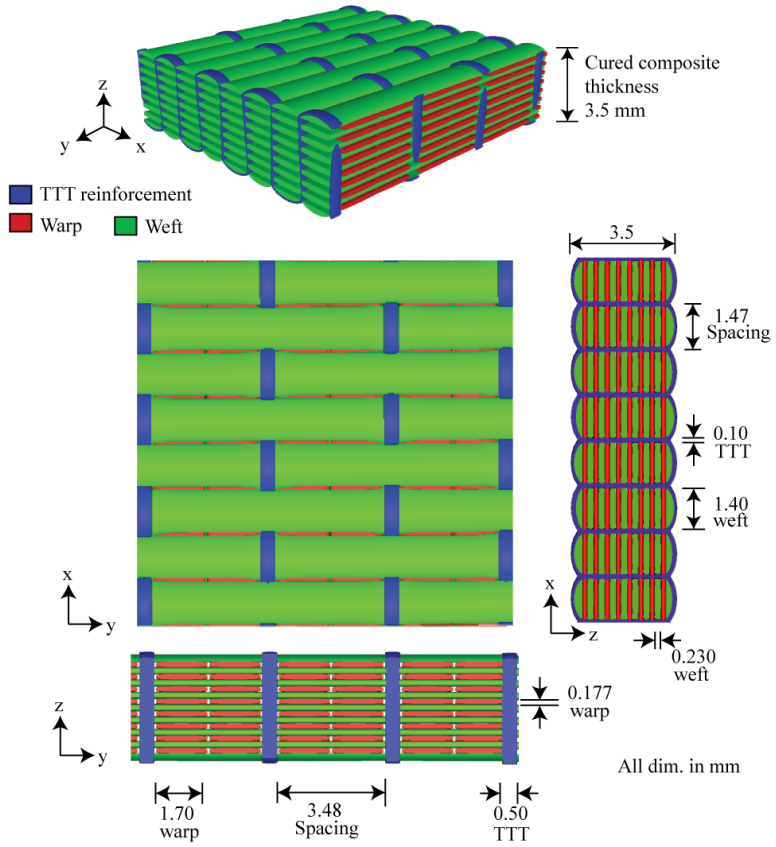

Figure 1: Sketch of 3D orthogonal woven carbon composites.

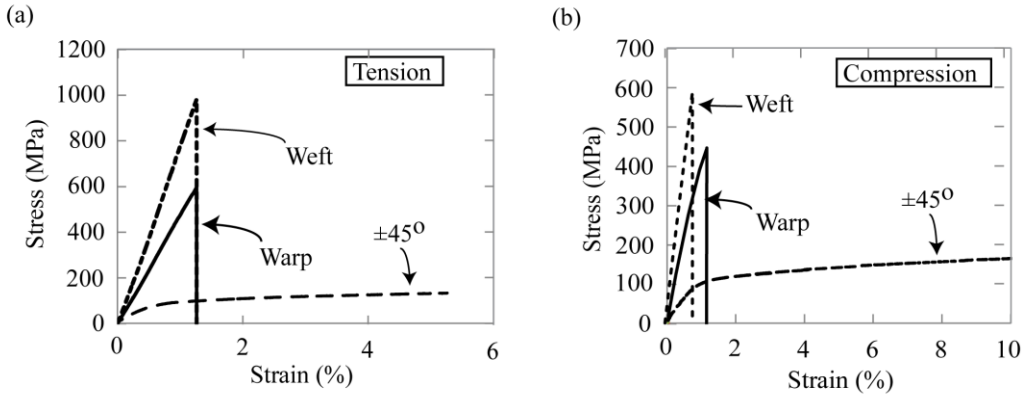

Figure 2 : Quasi-static stress strain relationships for 3D woven carbon composite material for (a) tension and (b) compression.

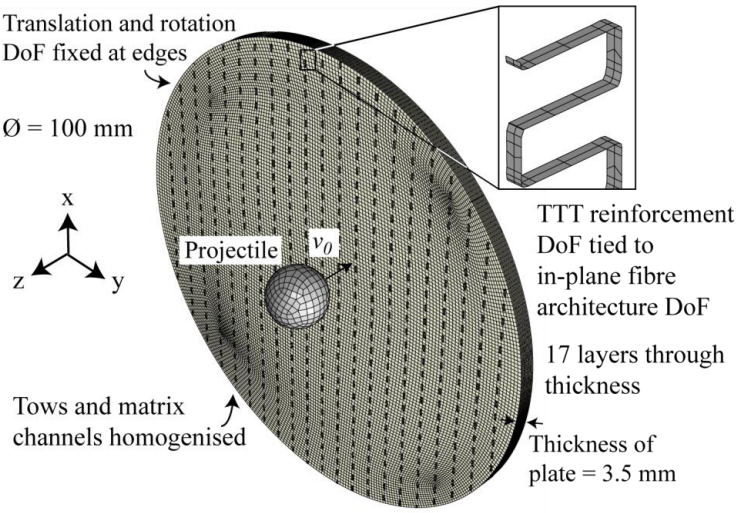

Figure 3: Meshed geometry for singular-hit ballistic impact simulations upon 3D woven composite circular plates.

4 RESULTS AND DISCUSSION

Numerical predictions of singular impact events upon 3D woven composite circular plates are now presented. Figure 3 presents a sketch of the meshed geometry of the singular-hit ballistic impact simulation upon 3D woven composite circular plates. To investigate the response of the composite material under ballistic impact, singular impact simulations with and without the presence of the TTT reinforcement were undertaken. Through this, the role of the through-the-thickness reinforcement during ballistic impact testing can be elucidated.

4.1 Deformed configuration and stress distribution

The two material types demonstrate different damage and deformation mechanisms during penetration. In short, the presence of the TTT-reinforcement caused an 8% increase in the predicted ballistic limit of the composite plate, i.e. an increase from V_L = 152.5 ms^{-1} without TTT reinforcement to V_L = 165.0 ms^{-1} inclusive of TTT reinforcement. Plates with and without TTT reinforcement were predicted to experience longitudinal fibre fracture throughout the thickness of the plate under the projectile strike location at a velocity of approximately $v_0 = 0.6\,V_L$. This agrees well with ballistic impact testing of CFRP plates presented by Kandan et al. [6]. The predicted mechanisms demonstrated during the test will now be described.

During the initial stages of ballistic impact, the FE model reveals the propagation of a high velocity tensile stress wave from the projectile impact location, travelling towards the clamp. This tensile stress wave primarily follows the in-plane fibre orientation, and travels at the longitudinal speed of sound within the material. This is shown clearly in the first montage image for the prediction of longitudinal tensile stress during a rigid spherical impact upon both 3D woven composite and UD-laminate composite in Figure . As described by analytical models [7], the inward flow of material towards the centre point allows the initial bulging of the plate underneath the projectile. This tensile stress wave was predicted to have the same velocity and magnitude with and without the presence of the binder. This is demonstrated with the first image of the montages presented in Figure (a) and (b). The stress within the back-face of the plates is presented here as it gives an indication of the transferal of stress throughout the thickness of the plate.

A lower velocity bending wave then propagates radially out from the impact location, travelling towards the clamped edges. The velocity of the bending wave is increased along the fiber direction, resulting in a characteristic ‘diamond’ shape pattern of stresses and deflections. This coincides well with the experimentally measured back-face deflection of composite plates under spherical projectile impact reported by Kandan et al. [6], and for numerical simulations of anisotropic stress wave propagation of a 3D woven composite material presented by Ghosh and De [8]. Figure 4(a) presents

the longitudinal stress within the through-thickness reinforcement at time t = 125 μs after the moment of projectile impact. Stress concentrations were predicted within the though-thickness reinforcement, coinciding with the transient position of the propagating bending wave. Extensive compressive fibre damage within the through-thickness reinforcement is predicted under the projectile location, in particular for the TTT reinforcement crowns. In the 3D woven composite, stress transferal from the in-plane fibre architecture to the through-thickness reinforcement was demonstrated. This causes a significant reduction in in-plane longitudinal tensile stress throughout the plate, and also local reductions in stress at the positions of the TTT reinforcement. This is demonstrated by a comparison of the predicted longitudinal stress distribution with and without the through-thickness reinforcement in Figure 4 (a) and (b). The predicted longitudinal stress within the TTT reinforcement is shown in Figure 4 (c). Transient stress transferal to the TTT reinforcement is demonstrated, following the location of the bending wave.

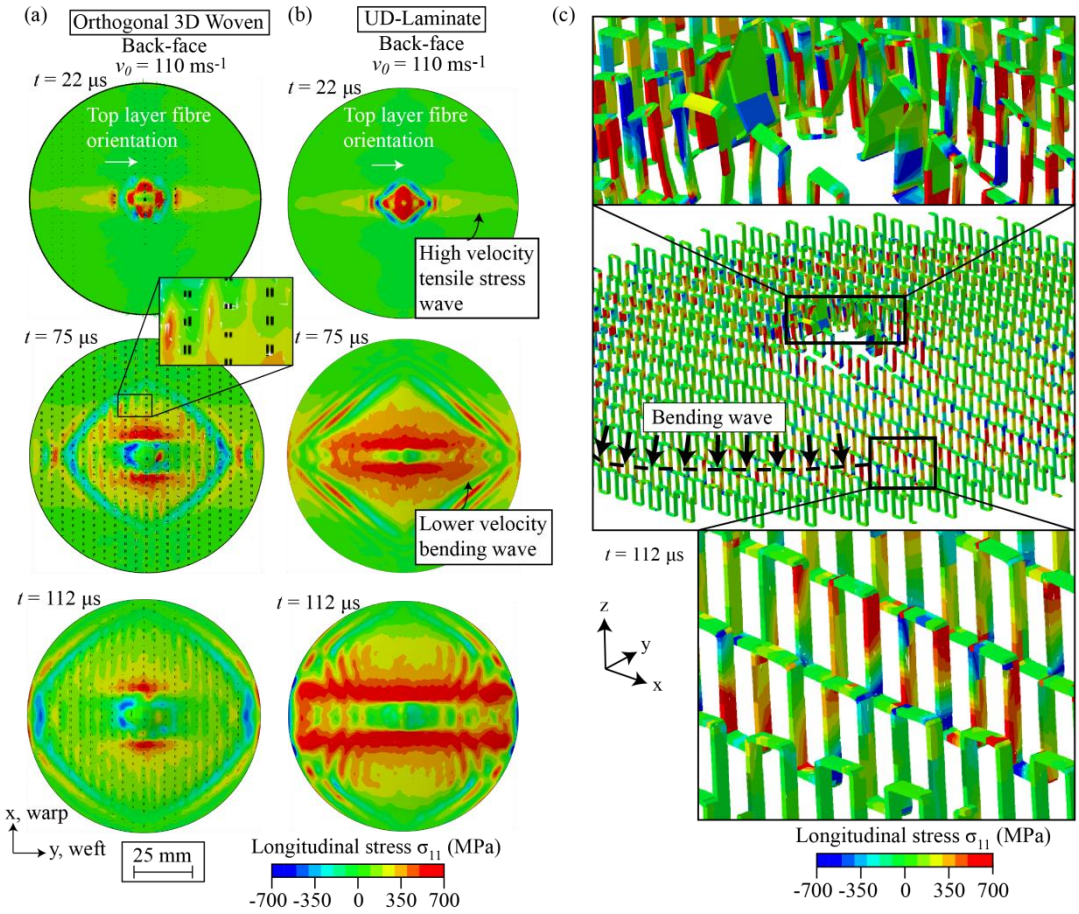

Figure 4 : Predicted transient longitudinal tensile stress field on back-face of plate impacted by a singular rigid spherical projectile of velocity $v_0 = 110\ \text{ms}^{-1}$ for (a) Orthogonal 3D woven composite (b) Equivalent UD-laminate composite. Time t is the moment of projectile impact upon plate. (c) Predicted longitudinal stress in the through-thickness reinforcement at time after impact t = 112 μs of impact velocity $v_0 = 110\ \text{ms}^{-1}$.

4.2 Equivalent UD-laminate clamped plate deformation and penetration mechanisms

The sequence of penetration mechanisms predicted by the numerical calculations for the equivalent UD-laminate material is illustrated in Figure 5, and outlined below:

i. as the projectile makes contact with the plate, a tensile stress wave develops within the material, travelling along the fibre direction out towards the clamped edges. This allows for the initial deformation of the plate.

ii. a travelling bending hinge propagates out from the impact location, travelling with a greater velocity along the principal fibre directions. This causes a growing cone of out-of-plane deformation underneath the projectile location.
iii. delamination damage then becomes significant. Due to the transferal of momentum, it is seen to be more prominent in the bottom ply of the composite. Simultaneous to this, cross shaped fibre fractures develop, propagating away from the impact location and brittle cone fibre fracture occurs underneath the projectile location.
iv. as the impact event continues, cross-shaped fractures increase in size, and combined with the bending deformation of delaminated plies, allows for the pass-through of the projectile.

The separate events of the penetration; the formation of the initial brittle fracture cone underneath the projectile, the propagation of cross-splits, and the bending deformation of delaminated plies, naturally leads to a case in which the projectile has enough kinetic energy to active one or two modes, but not to penetrate. The finite element model captures a specific velocity, i.e. v_0= 150 ms^{-1}, in which the projectile becomes trapped within the material. This transition point between projectile rebound and penetration, occurs at kinetic energies high enough to cause fibre fracture, yet not high enough for plate deformation allowing for complete projectile pass-through. The damage modes, and the transition point between rebound and penetration phenomenon, corresponds well to that recorded by experimental testing of CFRP plates by Kandan, et al. [6]. Figure 5 presents a sketch of a cross section of the plate showing the penetration mechanisms described here, along with a montage of the penetration event predicted by the FE method. The contour of Figure5(b) shows the onset of longitudinal fibre tensile damage. The finite element prediction clearly demonstrates the cross-shaped damage distribution, along with bending of plies to allow for projectile pass-through. Fully damaged elements have been removed from the visualisation to improve clarity. Figure 5 (c) presents a side-by-side comparison of cross-sectional x-ray image of an impact of velocity v_0 = 206 ms^{-1} upon a [0°/90°$_7$/0°] UD-laminate composite as presented by Karthikeyen Kandan PhD thesis (2013) [9] and numerically predicted response of the equivalent UD-laminate material undergoing an impact velocity of v_0 = 155 ms^{-1}. The UD-laminate material demonstrates spring back of proximal laminae, and extensive delamination remote from the projectile strike position. This response is different in the case inclusive of the TTT reinforcement, as presented later in Figure 6.

4.3 3D woven composite plates deformation and penetration mechanisms

FE simulations of a penetration event of a 3D woven composite material impacted by a projectile velocity of $v_0 = 170$ ms^{-1} were undertaken in order to ascertain the deformed configuration and damage mechanisms during penetration. Comparisons are made without the presence of the TTT reinforcement. Figure 6 (a) and (b) presents a sketch of the mechanisms and the numerically predicted longitudinal fibre damage contours during penetration, respectively. The main stages of the event are outlined below:

i. The propagation of a longitudinal tensile stress wave along the principal fibre direction allows for the initial cone formation. This is identical to the UD-laminate material.
ii. Membrane stretching occurs and a bending wave emanates from the impact location and travels towards the clamped edges. This is identical to the UD-laminate material.
iii. A combination of compressive fracture of through-thickness reinforcement and tensile fracture of longitudinal fibre reinforcement occurs under the projectile location. The in-plane tensile fibre fracture begins on the surface distal to projectile strike and propagates upwards towards the strike face.
iv. Localised deformation and damage of in-plane plies and through-thickness reinforcement around the projectile location allows for projectile penetration. Delamination within the material is restricted from under the projectile strike location up until the nearest un-damaged TTT reinforcement tow.

The final image shows the predicted asymmetric damage as the TTT reinforcement tow is fractured on the right hand side, causing a change in the local deformation. Capturing asymmetrical damage such as this is one of the key advantages of explicitly modelling the binder. Images of the FE

prediction of an impact of velocity $v_0 = 170\,\mathrm{ms}^{-1}$, presented in Figure 6 (b), clearly demonstrate damage concentrated under the projectile. This is different to the cross-shaped fracture and bending deformation predicted with the UD-laminate material. In regards to the back surface of the plates, the damage was predicted to propagate more favourably along the direction of the TTT reinforcement, as opposed to the fibre orientation. Figure 6(c) presents a cross-sectional view of the numerically predicted response of the 3D woven composite plate undergoing an impact of velocity 170 ms^{-1}. Delamination was shown to be suppressed by the presence of the TTT reinforcement.

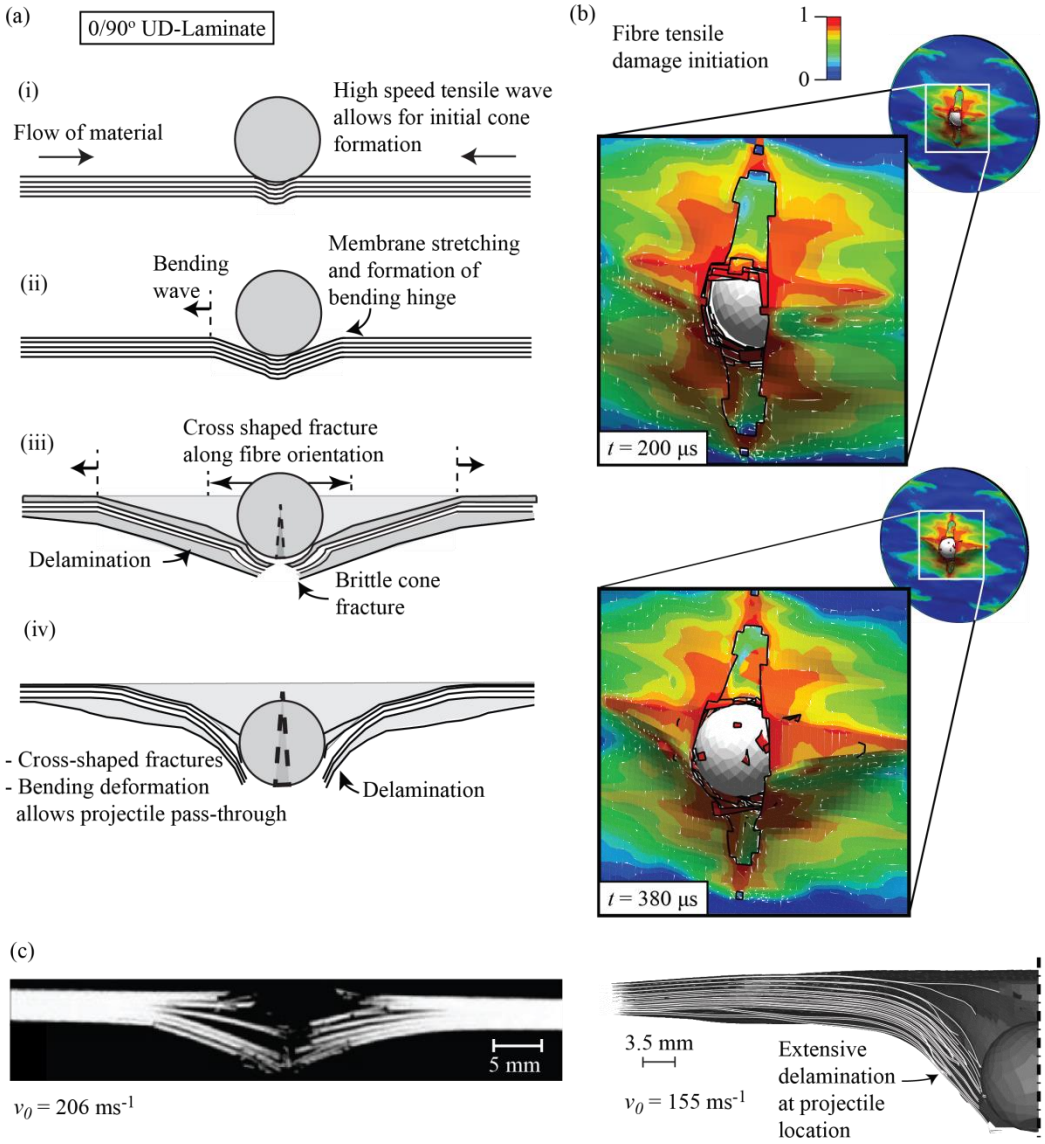

Figure 5: (a) Sketch of penetration mechanisms demonstrated by FE predictions of ballistic penetration event v_0 = 155 ms^{-1}: (i) inward flow of material allowing for initial bulging of plate, (ii) membrane stretching and formation of travelling bending hinge, (iii) brittle cone fracture and formation of cross shaped fracture of fibre reinforcement following principal fibre direction (iv) development of cross-shaped fibre fracture and wide-spread bending deformation of plate allowing for projectile pass-through. (b) montage of penetration event with contour showing longitudinal fibre damage initiation. A value of 1 indicates the onset of damage. (c) comparison of cross section of penetrated UD-laminate sample. Left: [0°/90°$_7$/0°] layup composite impacted at 206 ms^{-1} presented in Karthikeyan Kandan PhD Thesis (2013) [9]. Right: This study, FE simulation of equivalent UD-laminate clamped plate as shown in (b).

4.4 Fiber damage distribution

Figure 7 (a) and (b) presents the predicted tensile fibre damage initiation on the front-face of composite laminate plates undergoing ballistic impact of v_0 = 110 ms^{-1} at time after impact t = 225 μs with and without the presence of TTT reinforcement, respectively. A damage initiation value of 1 indicates the onset of damage of elements. The time chosen corresponds to the time at which the damage within the plates has fully developed for both cases. The top surface ply fibres are orientated along the y-direction (weft). The stress transferal from the in-plane fibre architecture to the through-thickness reinforcement effectively acts to reduce the fibre damage in the plate remote from the impact location; concentrating damage to the impact location. This has the effect of resisting the cross-shaped damage mode, reducing plate bending deformation. The tensile fibre damage was predicted to propagate more significantly in the direction of the TTT reinforcement for the 3D woven sample, and along the in-plane fibre orientation for the UD-laminate.

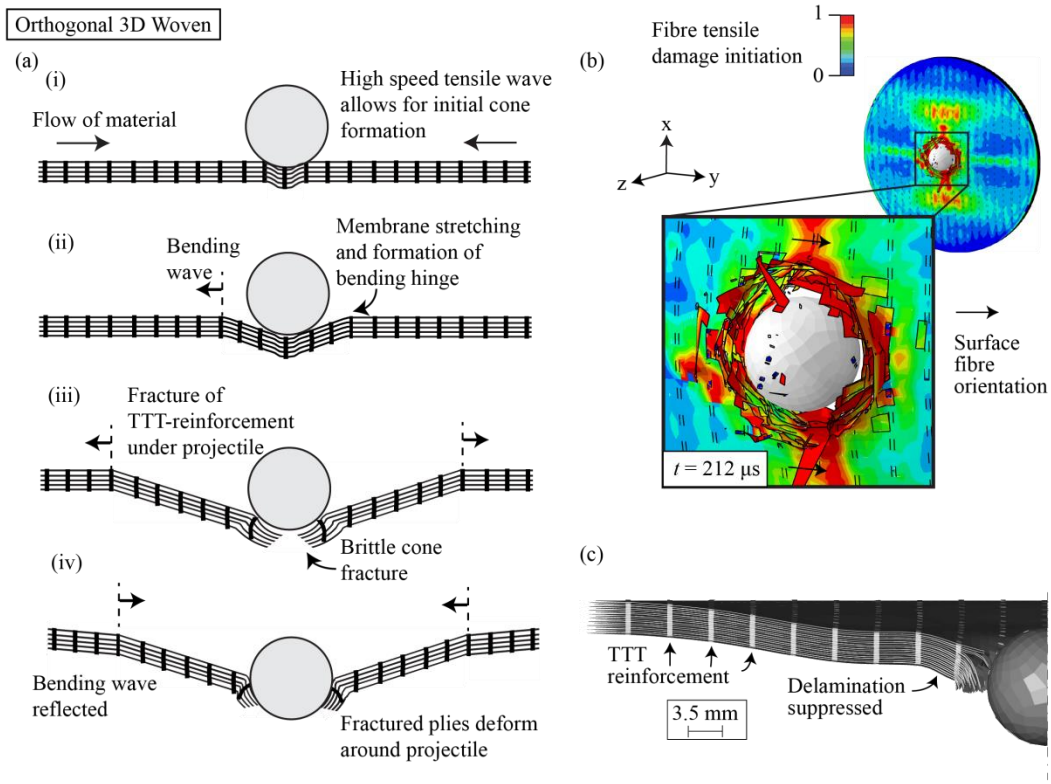

Figure 6: (a) Predicted mechanisms of deformation and penetration of orthogonal 3D woven composite material undergoing impact v_0 = 170 ms^{-1}: (i) inward flow of material allowing for initial bulging of plate, (ii) membrane stretching and formation of travelling bending hinge, (iii) fracture of TTT-reinforcement under projectile and brittle cone shaped fracture of in-plane fibre architecture, (iv) localised deformation and damage of in-plane fibre architecture allowing for projectile penetration, (b) Predicted deformed configuration and locations of initiation of tensile fibre damage of 3D woven composite material. A value of 1 indicates the onset of longitudinal tensile damage. (c) Cross-sectional image of the numerically predicted response of the 3D woven composite plate sample subjected to impact velocity v_0 = 170 ms^{-1}.

4.5 Coefficient of restitution

Predictions of both the 3D woven and equivalent UD-laminate material reveal a progressive increase of inelastic processes, predominantly of material damage, with increasing velocity of projectile impact. Inelastic processes within composite plates subjected to ballistic impact can be quantified by the ratio of input velocity and rebound projectile velocity. This ratio is referred to as the

coefficient of restitution. Effectively, this ratio quantifies the energy loss during the impact event due to frictional dissipation, and material damage.

Figure8 presents the predicted coefficient of restitution e as a function of the normalised impact velocity $\bar{v}_0$. The coefficient of restitution is defined as $e \equiv -v_R / \bar{v}_0$, where v_R is the rebounded steady-state velocity of the projectile after the impact event and the impact velocity is normalised against the predicted ballistic limit of the plate, i.e. $\bar{v}_0 \equiv v_0 / V_L$, where V_L is the ballistic limit. Both material types exhibit a rapid drop-off of the predicted coefficient of restitution at the same normalised impact velocity $\bar{v}_0 \approx 0.95$. This corresponds well with the ballistic impact experimental testing of UD-laminate plates as presented by Kandan, et al. [6]. The 3D woven material is shown to have approximately a 25% increase in the coefficient of restitution in comparison with the equivalent UD-laminate material within the normalised velocity range: $0.35 \leq \bar{v}_0 \leq 0.85$.

A comparison between the predicted response of the composite laminate plates and experimentally recorded coefficient of restitution as a function of normalised impact velocity [9] reveals the stark difference between material response. The metallic plate exhibits high levels of work done within the material due to plastic deformation, causing a greatly reduced coefficient of restitution. On the other hand, the elastic-brittle nature of fibre-reinforced composites leads to a higher value of coefficient of restitution.

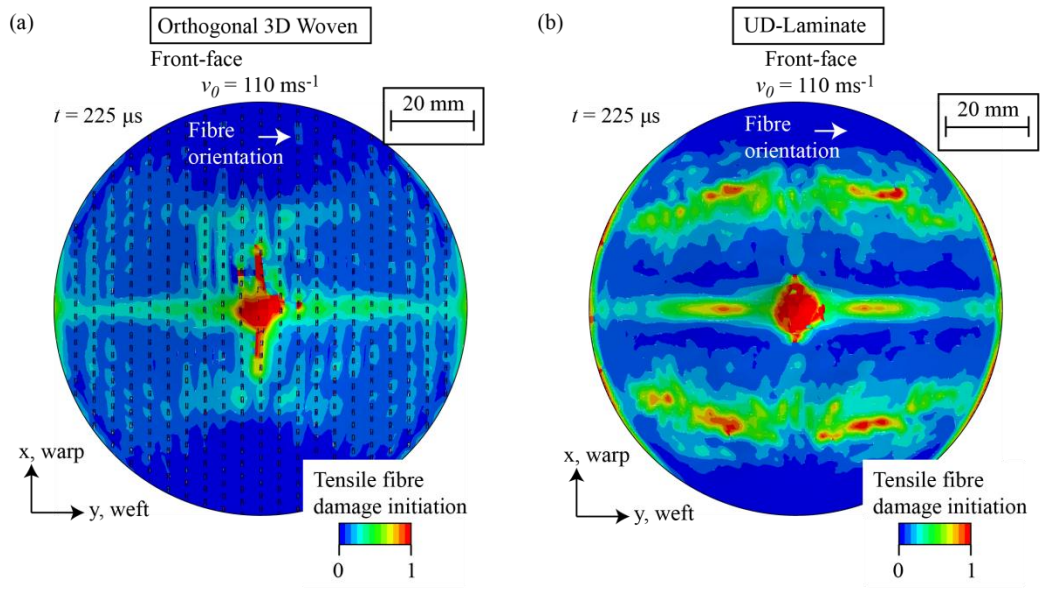

Figure 7: (a) and (b) Predicted tensile fibre damage initiation on the front-face of composite laminate beams undergoing ballistic impact of v_0 = 110 ms^{-1} at time after impact t = 225 µs for material with and without through-thickness reinforcement, respectively. Time t = 0 corresponds to the moment of projectile impact on plate. A damage initiation value of 1 indicates the onset of damage of elements. Top ply fibres orientated along the y-direction (weft).

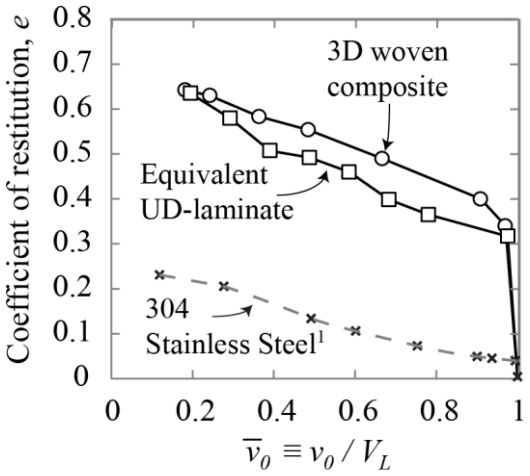

Figure 8: The predicted coefficient of restitution *e* as a function of the normalised impact velocity $\bar{v}_0 \equiv v_0 / V_L$ for the 3D woven composite and equivalent UD-laminate material. For comparative purposes, also presented is the experimentally recorded coefficient of restitution as a function of normalised impact velocity for a 304 stainless steel plate by Kandan et al.[9].

ACKNOWLEDGEMENTS

The authors acknowledge the support from the Engineering and Physical Sciences Research Council, UK (EPSRC EP/P505658/1 and EP/K503101/1) and the Royal Society (a charity registered in England with number 207043) through Research Grant Scheme. They also acknowledge the use of the High Performance Computing facility at the University of Nottingham for finite element calculations.

REFERENCES

[1] Mines RA, McKown S, Birch RS. Impact of aircraft rubber tyre fragments on aluminium alloy plates: I—Experimental, *International Journal of Impact Engineering*, **34**(4), 2007, pp. 627-46 (doi: 10.1016/j.ijimpeng.2006.02.005).

[2] Mouritz AP, Bannister MK, Falzon PJ, Leong KH. Review of applications for advanced three-dimensional fibre textile composites. *Composites Part A: applied science and manufacturing*, **30**(12), 1999, 1445-61(doi.org/10.1016/S1359-835X(99)00034-2).

[3] Turner P, Liu T, Zeng X, Dynamic response of orthogonal three-dimensional woven carbon composite beams under soft impact. *Journal of Applied Mechanics*, **82**(12), 2015, pp. 121008. (doi: 10.1115/1.4031455).

[4] Hashin Z, Failure criteria for unidirectional fiber composites. *Journal of applied mechanics*, **47**(2), 1980, pp.329-334. (doi:10.1115/1.3153664)

[5] Matzenmiller AL, Lubliner J, Taylor RL, A constitutive model for anisotropic damage in fiber-composites. *Mechanics of materials*. **20**(2), 1995, pp.125-52. (doi.org/10.1016/0167-6636(94)00053-0).

[6] Karthikeyan K, Russell B, Deshpande V, Fleck N. Multi-hit armour characterisation of metal-composite bi-layers. *Journal of Mechanics of Materials and Structures*. **7**(7), 2013, pp. 721-34. (doi: 10.2140/jomms.2012.7.721)

[7] Phoenix, S.L. and P.K. Porwal, A new membrane model for the ballistic impact response and V 50 performance of multi-ply fibrous systems. *International Journal of solids and structures*, **40**(24), 2003, pp. 6723-6765. (doi.org/10.1016/S0020-7683(03)00329-9).

[8] Ghosh, R. and S. De, Z-fiber influence on high-speed penetration of 3D orthogonal woven fiber composites. Mechanics of materials, **68**, 2014, pp. 147-163. (doi.org/10.1016/j.mechmat.2013.06.008)

[9] Kandan, K., *Dynamic Response of Polyethelene Composites*. PhD Thesis, University of Cambridge, 2013